

Influence of ageing on Raman spectra and the conductivity of monolayer graphene samples irradiated by heavy and light ions

A. Butenko,¹ E. Zion,¹ Yu. Kaganovskii,² L. Wolfson,² V. Richter,¹ A. Sharoni,¹ E. Kogan,² M. Kaveh,² and I. Shlimak²

¹*Institute of Nanotechnology and Advanced Materials, Bar-Ilan University, Ramat Gan 52900, Israel*

²*Jack and Pearl Resnick Institute, Department of Physics, Bar-Ilan University, Ramat Gan 52900, Israel*

(Dated: April 5, 2024)

The influence of long-term ageing (about one year) on the Raman scattering (RS) spectra and the temperature dependence of conductivity has been studied in two series of monolayer graphene samples irradiated by different doses of C^+ and Xe^+ ions. It is shown that the main result of ageing consists of changes in the intensity and position of D- and G- and 2D-lines in RS spectra and in an increase of the conductivity. The observed effects are explained in terms of an increase of the radius of the “activated” area around structural defects.

PACS numbers: 73.22.Pr, 72.80.Vp

I. INTRODUCTION

Ion irradiation is widely used for introducing defects and disorder in graphene films in order to modify their physical properties (see, for example,¹⁻⁴). The measurement of the Raman scattering (RS) spectra is considered an effective tool for probing the structure of disordered graphene and the density of introduced defects⁵⁻⁸. Typical RS spectra for disordered graphene consist of three main lines. The D-line at 1350 cm^{-1} is related to the inter-valley double resonant process in graphene in the vicinity of a lattice defect (edge, vacancies.) The 2D-line at 2700 cm^{-1} , is related to an inter-valley two phonon mode, characteristic of the perfect crystalline honeycomb structure. The G-line at 1600 cm^{-1} is common for different carbon-based materials, including carbon nanotubes and graphite. The appearance of the D-peak is ascribed to the breathing of carbon hexagons at the borders of the crystallite areas or in the vicinity of a structural defect, reflecting the loss of translational symmetry⁵. The intensity of the D-line is used (usually in the form of the dimensionless ratio of intensities of the D- and G-lines, I_D/I_G) as a measure of disorder in the graphene layer. In addition, a few minor lines connected with different modes of phonons can be seen in disordered samples: D'-line (1620 cm^{-1}), D+D'-line (2970 cm^{-1}) and D+D"-line (2450 cm^{-1}). The positions of all lines are given for 532 nm excitation laser.

The main aim of the present study is the investigation of the influence of long-term ageing (about one year) on properties of monolayer graphene samples irradiated by different dose of heavy and light ions. From one side, the ambient atmosphere is not fully reproducible in different places and laboratories, but from the other side, most devices are kept in ambient atmosphere, therefore this investigation might be of interest for specialists in graphene-based devices.

II. SAMPLES

In our previous studies⁹⁻¹¹, we reported the results of the investigation of the optical (RS) and the electrical (conductivity and magnetoresistance) properties of monolayer graphene samples irradiated by different doses Φ of carbon ions C^+ with energy 35 keV. Six series of micro-samples ($200 \times 200\text{ }\mu\text{m}$) provided with two metal contacts were prepared by means of electron-beam lithography on a common large-scale ($5 \times 5\text{ mm}$) monolayer graphene specimen supplied by “Graphenea” company. Monolayer graphene was produced by CVD on copper catalyst and transferred to a 300 nm SiO_2/Si substrate using wet transfer process. Graphene film of such a large size was not a monocrystalline. It looks like a polycrystalline film with the average size of microcrystals about a few microns⁹. In the present study, we also include the results obtained on a series of monolayer graphene samples irradiated by heavy ions Xe^+ with the same energy $E = 35\text{ keV}$. In this series, micro-samples were not fabricated, six areas $2 \times 1\text{ mm}$ of the whole specimen $5 \times 5\text{ mm}$ were irradiated separately with different doses of Xe ions.

III. RAMAN SCATTERING

In the RS spectra measurements, excitation was realized by the laser beam with $\lambda = 532\text{ nm}$ and power less than 2 mW to avoid heating and film destruction. Reproducibility was verified by repeated measurements in different areas and different samples of the same group.

Figure 1 shows the RS spectra for both series of samples immediately following irradiation (a, c) and after long-term ageing (b, d). The changes of the main lines of the RS with increasing Φ are as expected: in non-irradiated samples (0) the intensity of the “defective” D-line is small or absent which demonstrates the good quality of the initial monolayer graphene specimen. In-

creasing the dose of the irradiation Φ causes the D-line to increase and then broaden and decrease, while the 2D-line monotonically decreases and disappears. To compare results of irradiation by different ions, one plots the ratio I_D/I_G and I_{2D}/I_G as a function of the density of structural defects N_D , which is proportional to the dose of irradiation Φ , $N_D = k\Phi$. The coefficient k depends on the energy E and the mass M of the irradiated ions and reflects the average fraction of carbon vacancies in the graphene lattice per ion impact. A computer simulation of this process was performed in Ref.¹². On the basis of this simulation, we plot in Fig. 2 the dependence of k as a function of M (in atomic mass units, amu) for different E .

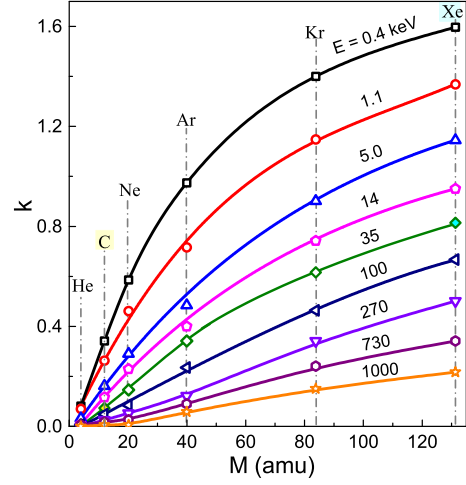


FIG. 2. (Color online) Dependence of k on the ion mass M for different energies E shown in keV. Masses of some ions are indicated by vertical dotted lines.

One can see in Fig. 2 from the curve $E = 35$ keV that for C^+ ions ($M = 12$) $k \approx 0.06-0.08$, whereas for Xe^+ ($M = 131$), $k \approx 0.8$. Therefore, to equalize the density of the introduced defects N_D , we used for Xe^+ one order of magnitude smaller doses Φ than for C^+ ions. The dependence of I_D/I_G and I_{2D}/I_G for both series of samples after irradiation is shown in Fig. 3. One can see that the experimental data for the C- and Xe- series are indeed close but not identical.

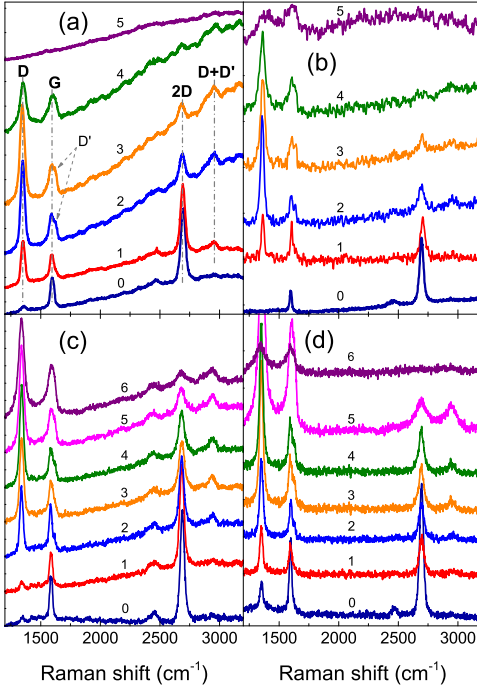


FIG. 1. (Color online) Raman scattering spectra for two series of samples irradiated with C^+ ions (a, b) and Xe^+ ions (c, d): (a, c) - after irradiation, (b, d) - after long-term ageing. For C-series, Φ in units of 10^{14} cm^{-2} : 0 - 0 (initial), 1 - 0 (non-irradiated, but after E-beam lithography [9]), 2 - 0.5, 3 - 1.0, 4 - 2.0, 5 - 10; for Xe-series, Φ in units of 10^{13} cm^{-2} : 0 - 0 (initial), 1 - 0.15, 2 - 0.3, 3 - 0.5, 4 - 1.0, 5 - 2.0, 6 - 4.0.

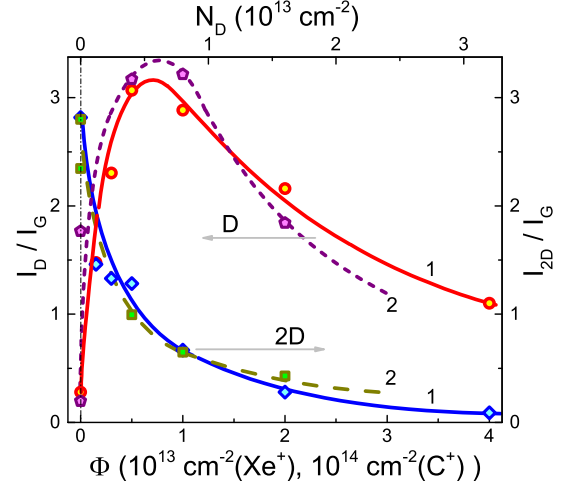


FIG. 3. (Color online) The ratio I_D/I_G and I_{2D}/I_G for “irradiated” samples for Xe- (1) and C- (2) series as a function of Φ (in units of 10^{13} cm^{-2} for Xe^+ and 10^{14} cm^{-2} for C^+). The upper scale shows the density of introduced defects N_D common for both series.

Long-term ageing leads to changes in the RS spectra. Figure 4 shows the spectra for some “irradiated” and “aged” samples from the Xe-series. One can see that the intensity of D-lines in the “aged” samples is stronger for weakly irradiated samples but weaker for strongly irra-

diated samples, while the 2D-lines are always weaker in the “aged” samples.

To explain the changes in the RS induced by long-term ageing, we plot in Figs. 5a,b the ratio I_D/I_G as a function of the mean distance between defects, $L_D \approx N_D^{-1/2}$. At large L_D (small Φ), the ratio I_D/I_G increases with decreasing L_D , passes through a maximum and then rapidly decreases. Such non-monotonic behavior is common for many experimental observations^{5–9} and agrees with the theoretical model¹³ based on the assumption that a single ion impact leads to the formation of a defect characterized by two length scales r_S and r_A ($r_A > r_S$), which are the radii of two circular areas surrounding the defect (see insert in Fig. 5). The area S within the shorter radius r_S around the impact point is structurally disordered. In the A -area (“activated” area) between r_A and r_S , the lattice structure is preserved, but the proximity to the impact point causes a breakdown of the selection rules and gives rise to the “defective” D-peak. The 2D-peak, which is characteristic for a perfect graphene lattice, can be generated only if the electron-hole excitation occurs outside the A -area. Increasing the irradiation dose Φ obviously results in an increase of the D-line intensity and a decrease of the 2D-line intensity. Increasing of Φ leads to a decrease of $L_D \approx (k\Phi)^{-1/2}$ and when L_D becomes shorter than r_A , the A -areas begin to overlap with each other and with S -areas. As a result, I_D/I_G passes through a maximum and then decreases.

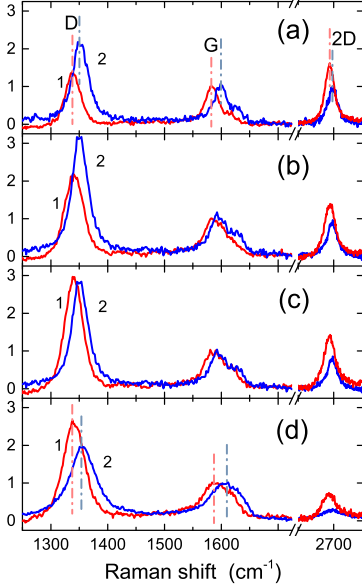


FIG. 4. (Color online) Comparison of the normalized RS spectra in “just irradiated” (1) and “aged” (2) samples from Xe-series with different irradiation dose Φ (in units of 10^{13} cm^{-2}): $a - 0.3$, $b - 0.5$, $c - 1.0$, $d - 2.0$. Intensity of G-line is taken as 1.

The solid and dotted lines in Fig. 5 represent the theoretical expression for the dependence of $I_D/I_G(L_D)$ that was obtained in Ref.¹³ and modified in Ref.⁹:

$$I_D/I_G = C_A e^{-\pi r_S^2/L_D^2} [1 - e^{-\pi(r_A^2 - r_S^2)/L_D^2}] + C_S [1 - e^{-\pi r_S^2/L_D^2}] \quad (1)$$

Here, the parameter C_A is the maximal possible value of the I_D/I_G ratio in graphene, which could be attained for the situation in which no damage occurred to the hexagonal network of carbon atoms, and C_S is the I_D/I_G value in the highly disordered limit⁵.

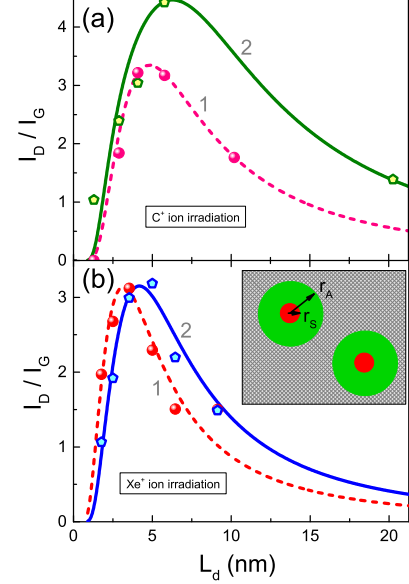


FIG. 5. (Color online) I_D/I_G as a function of L_D for C-series (a) and Xe-series (b) of samples. Curves 1 and 2 show the best fit of theoretical curve Eq. (1) for “irradiated” and “aged” samples, correspondingly. Insert shows schematics of radiation defects of two length scales (see text).

The best fit of the experimental data shown in Fig. 5 is given by the solid and dashed lines, corresponding to the following values of the adjustable parameters in Eq. (1):

C-series		Xe-series	
$C_S = 0, C_A = 5.4$,		$C_S = 0, C_A = 4.9$,	
“irradiated”	“aged”	“irradiated”	“aged”
$r_S(\text{nm}): 1.55$	1.35	1.0	1.3
$r_A(\text{nm}): 4.1$	6.4	2.8	3.7

TABLE I. Adjustable parameters of Eq.(1) determined from the best fitting with experimental data shown in Fig. 5.

Analysis of these data shows that the main effect occurs as a function of r_A . Comparison of “irradiated” samples before ageing shows that irradiation with relatively light ions (C^+) is characterized by a larger values of r_S and r_A than irradiation with heavy ions (Xe^+). This could be connected with existence of a backscattering in the case of bombardment of SiO_2 substrate by

C ions which are lighter than atoms in the substrate, in contrast to irradiation by heavy Xe ions.

Long-term ageing leads to an increase in r_A in both series. The increase of the square of A -area could be caused by the capture of molecules from the ambient atmosphere which can lead to increasing the Raman relaxation length $l = r_A - r_S$.⁵ This increase of r_A explains the different behavior of the D-line for weakly and strongly irradiated samples shown in Fig. 4. For weakly irradiated samples, the D-line increases because of the increase of the square of A -areas. However, the overlap of increased A -areas begins earlier, at a lower density of defects, which explains the decrease of the D-line in strongly irradiated samples.

One can see also from Fig. 4 that the peaks in the “aged” samples shift to higher frequencies (“blue shift”). The largest values of the blue shift are 18 and 14 cm^{-1} for the G- and D-peaks, respectively. There are several possible origins for the blue shift, including stress and the effects of doping¹⁴. The doping-based scenario agrees with the assumption that the increase of r_A in aged samples is caused by the capture of molecules from the ambient atmosphere.

IV. ELECTRICAL CONDUCTIVITY

In series of C^+ -irradiated samples, the temperature dependence of the conductivity σ and the resistivity $R = 1/\sigma$ were measured before ageing, after irradiation, and the results were reported in Refs.^{10,11}. It was shown that $\sigma(T)$ for sample 1 with a low density of defects, N_D , is accurately described in the framework of the weak localization (WL) model, whereby $\sigma(T) \sim \ln(T)$ and saturates at low T . The resistivity of more disordered samples 2,3,4 is governed by variable-range hopping (VRH), characteristic of strongly localized carriers. VRH is described by exponential laws: $R \sim \exp(T^{-p})$, with $p = 1/3$ at relatively high T (“Mott-law”) and $p = 1/2$ (“Efros-Shklovski law”) at low T . Measurements of $R(T)$ after ageing showed the increase of conductivity for all samples (Fig. 6).

On the first glance, increase of conductivity could be attributed to the doping due to capture of molecules from the ambient atmosphere. However, the term “doping” is more applicable to pristine or slightly disordered graphene when conductivity is realized by free charge carriers and can be changed by variation of the gate voltage in the field-effect-transistor (FET) geometry in both directions from the charge neutrality point^{15,16}. In our samples, variation of the gate voltage up to ± 80 V weakly changes the conductivity, so the charge neutrality point was not achieved. This is due to the fact, that conductivity in our disordered highly resistive graphene samples is realized by localized charge carriers^{10,11}. Localization is caused by the random potential relief, induced by the large density of negatively and positively charged defects. Increase of r_A can lead to smearing of

this relief, weakening of localization and corresponding increase of conductivity. Therefore an increase of r_A due to capture of molecules from the ambient atmosphere would be better described as “alteration” rather than “doping”.

Figure 6 shows that before ageing, $R(T)$ for “irradiated” samples 2 and 3 is governed by the VRH mechanism which corresponds to a straight line when plotted as $\log(R)$ vs. $T^{-1/3}$ (curves 2a and 3a in Fig. 6a), while after ageing, the reduced resistance deviates from a straight line and even shows a tendency to saturation at low T (curves 2b and 3b in Fig. 6a). As a result, the conductivity of these samples is better described by a plot of WL $\sigma(T) \sim \ln(T)$ (Fig. 6b). The transition from strong to weak localization after ageing can be explained by a softening of the random potential relief due to an increase of r_A . For strongly irradiated sample 4, the dependence $R(T)$ after ageing still exhibits the VRH mechanism even though the resistivity decreases.

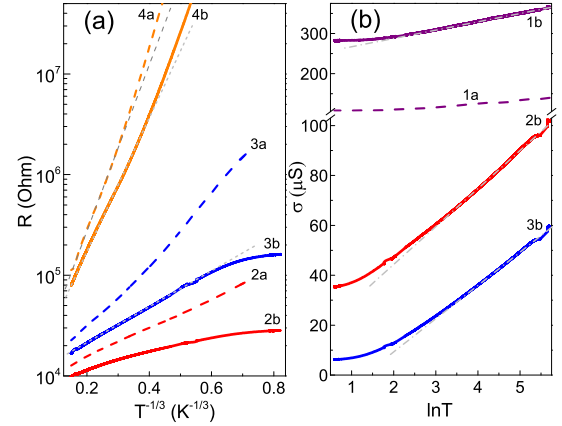


FIG. 6. (Color online) Temperature dependence of resistivity R and conductivity $\sigma = 1/R$ of C^+ -irradiated samples plotted on the scale appropriate for VRH regime (a) and for WL regime (b). Numbers near curves correspond to the numbers of samples in Fig. 1(a,c): 1a, 2a, 3a, 4a – “irradiated” samples, 1b, 2b, 3b, 4b – “aged” samples.

The influence of ageing on the Raman scattering spectra and the conductivity in graphene layers had not been studied earlier. There were only measurements of the Raman signal from aged nanographite¹⁷ and from organic molecules absorbed on the aged graphene¹⁸. In Ref.¹⁶, an increase of resistance after ageing in ambient atmosphere was observed in field effect transistors made from pristine graphene. In Ref.¹⁹, the influence of ageing was studied on the electrical properties of graphene-based transparent flexible electrodes.

In this study, we show that long-term ageing of pristine and ion-irradiated monolayer graphene samples kept in ambient atmosphere leads to changes in the intensity and a blue-shift in the position of the D-, G- and 2D-

lines in the RS spectra and to an increase of the electrical conductivity. Our explanation is based on the notion of “activated” areas around structural defects in graphene. We suggest that the radius of this “activated” areas increases in the process of ageing which is caused by capturing molecules from the ambient atmosphere.

V. ACKNOWLEDGEMENTS

One of the authors (E.K.) cordially thanks Center for Theoretical Physics of Complex Systems, Institute for

Basic Science (IBS), Daejeon, Republic of Korea for the hospitality during his stay.

-
- ¹ Quan Wang, Wei Mao, Daohan Ge, Yanmin Zhang, Ying Shao and Naifei Ren, *Appl. Phys. Lett.* **103**, 073501 (2013).
 - ² Beidou Guo, Qian Liu, Erdan Chen, Hewei Zhu, Liang Fang and Jian Ru Gong, *Nano Lett.* **10**, 4975 (2010).
 - ³ Grant Buchowicz, Peter R. Stone, Jeremy T. Robinson, Cory D. Cress, Jeffrey W. Beeman, and Oscar D. Dubon, *Appl. Phys. Lett.* **98**, 032102 (2011).
 - ⁴ Gaurav Nanda, Srijit Goswami, Kenji Watanabe, Takashi Taniguchi, and Paul F.A. Alkemade, *Nano Lett.* **15**, 4006 (2015).
 - ⁵ M.S. Dresselhaus, A. Jorio, A.G. Souza Filho, and R. Saito, *Phil. Trans. R. Soc. A* **368**, 5355 (2010).
 - ⁶ Andrea C. Ferrari and Denis M. Basko, *Nature Nanotechnol.* **8**, 235 (2013).
 - ⁷ Ado Jorio, Marcia M. Lucchese, Fernando Stavale, Erlon H. Martins Ferreira, Markus V.O. Moutinho, Rodrigo B. Capaz, and Carlos A Achete, *J. Phys.: Condens. Matter* **22**, 334204 (2010).
 - ⁸ R. Saito, M. Hofmann, G. Dresselhaus, A. Jorio, and M.S. Dresselhaus, *Adv. Phys.* **60**, 413 (2011).
 - ⁹ I. Shlimak, A. Haran, E. Zion, T. Havdala, Yu. Kaganovskii, A.V. Butenko, L. Wolfson, V. Richter, D. Naveh, A. Sharoni, E. Kogan, and M. Kaveh, *Phys. Rev. B* **91**, 045414 (2015).
 - ¹⁰ Erez Zion, Avner Haran, Alexander V. Butenko, Leonid Wolfson, Yuri Kaganovskii, Tal Havdala, Amos Sharoni, Doron Naveh, Vladimir Richter, Moshe Kaveh, Eugene Kogan, and Issai Shlimmak, *Graphene* **4**, 45 (2015).
 - ¹¹ I. Shlimak, E. Zion, A.V. Butenko, L. Wolfson, Yu. Kaganovskii, A. Sharoni, A. Haran, D. Naveh, E. Kogan, and M. Kaveh, *Physica E* **76**, 158 (2016).
 - ¹² O. Lehtinen, J. Kotakoski, A.V. Krashennikov, A. Tolvanen, K. Nordlund, and J. Keinonen, *Phys. Rev. B* **81**, 153401 (2010).
 - ¹³ M.M. Lucchese, F. Stavale, E.H. Martins Ferreira, C. Vilani, M.V.O. Moutinho, Rodrigo B. Capaz, C.A. Achete, A. Jorio, *Carbon* **48**, 1592 (2010).
 - ¹⁴ A. Das, S. Pisana, B. Chakraborty, S. Piscanec, S. K. Saha, U. V. Waghmare, K. S. Novoselov, H. R. Krishnamurthy, A. K. Geim, A. C. Ferrari, and A. K. Sood, *Nat. Nanotechnol.* **3**, 210 (2008).
 - ¹⁵ M. Bruna, A. K. Ott, M. Ijas, D. Yoon, U. Sassi, A. C. Ferrari, *ACS Nano* **8**, 7432 (2014).
 - ¹⁶ S. Rumyantsev, G. Liu, W. Stillman, M. Shur, and A. A. Balandin, *J. Phys. Condens. Matter* **22**, 395302 (2010).
 - ¹⁷ Tatiana Makarova, Mauro Ricco, Daniele Pontiroli, Marcello Mazzani, Matteo Belli, and Angelo Goffredi, *Phys. Stat. Sol. (b)* **245**, 2082 (2008).
 - ¹⁸ Yingying Wang, Zhenhua Ni, Aizhi Li, Zainab Zafar, Yan Zhang, Zhonghua Ni, Shiliang Qu, Teng Qiu, Ting Yu, and Ze Xiang Shen, *Appl. Phys. Lett.* **99**, 233103 (2011).
 - ¹⁹ Yuanyuan Shi, Yanfeng Ji, Fei Hui, Hai-Hua Wu, and Mario Lanza, *Nano Research* **7**, 1820 (2014).